SIAM J. APPL. MATH.
Vol. 74, No. 1, pp. 40–59

PULSATILE VISCOUS FLOWS IN ELLIPTICAL VESSELS AND ANNULI: SOLUTION TO THE INVERSE PROBLEM, WITH APPLICATION TO BLOOD AND CEREBROSPINAL FLUID FLOW*

LUIGI C. BERSELLI†, FRANCESCA GUERRA‡, BARBARA MAZZOLAI‡, AND EDOARDO SINIBALDI‡

Abstract. We consider the fully developed flow of an incompressible Newtonian fluid in a cylindrical vessel with elliptical cross section, and in the annulus between two confocal ellipses. Since flow rate can actually be derived from measurements, we address the *inverse problem*, namely computing the velocity field associated with a given time-periodic flow rate. We propose a novel numerical strategy, which is nonetheless grounded on several analytical relations and which leads to the solution of systems of ordinary differential equations. We also report numerical results based on measured data for human blood flow in the internal carotid artery, and cerebrospinal fluid flow in the upper cervical region of the human spine. Our method holds promise to be more amenable to implementation than previous ones, based on challenging computation of Mathieu functions, especially for strongly elliptical cross sections. The main goal of this study is to provide an improved source of initial/boundary data, as well as a benchmark solution for pulsatile flows in elliptical sections. In addition to bio-fluid dynamics investigations, the proposed method can be applied to many problems in the biomedical field.

Key words. pulsatile laminar flow, elliptical vessel, inverse problem, cerebrospinal fluid flow, blood flow

AMS subject classifications. Primary, 76Z05; Secondary, 35Q30, 92C35

DOI. 10.1137/120903385

1. Introduction.

Pulsatile flows are driven by a time-periodic force, which is generally the pressure gradient. A remarkable case is that of heartbeat-driven, human physiological flows, including blood circulation [30] and, even if less directly, cerebrospinal fluid (CSF) flow [18]. In addition to bio-fluid dynamics, time-periodic flows are widely studied with regard to chemical-physics applications, mass and heat transfer problems, and peristaltic pumping [26]. However, in many cases of practical interest the pressure gradient is unknown or hardly measurable, while the flux—hereafter understood as a synonym of the flow rate—can actually be estimated through measurements. For instance, blood and CSF flow are commonly obtained by phase-contrast magnetic resonance imaging (MRI) or Doppler ultrasonography: Flow rate is obtained by somehow integrating low-space-resolution velocity measurements, which, however, are not resolved enough for determining the velocity profile. Anyway, measurement issues are outside the scope of this paper; hence the flux is assumed to be known with reasonable accuracy. Our study is mainly motivated by the fact that many portions of the vasculature are characterized by a rather elliptical cross section, due to the presence of surrounding organs. Moreover, the spinal subarachnoid space can be well approximated by an elliptical annulus [18]; CSF dynamics in such a domain is affected by pulsatility and plays a major role in the (still poorly understood)

*Received by the editors December 21, 2012; accepted for publication (in revised form) October 1, 2013; published electronically January 16, 2014.
http://www.siam.org/journals/siap/74-1/90338.html
†Dipartimento di Matematica, Università di Pisa, I-56127 Pisa, Italy (berselli@dma.unipi.it).
‡Center for Micro-BioRobotics@SSSA, Istituto Italiano di Tecnologia, I-56025 Pontedera, Italy (francesca.guerra@iit.it, barbara.mazzolai@iit.it, edoardo.sinibaldi@iit.it).

pathophysiology of many high-impact diseases, like syringomyelia and Chiari malformation [10].

In order to tackle realistic three-dimensional (3D) flow conditions within patient-specific geometries, a fully numerical approach is mandatory, which implies time-consuming simulations [9, 21, 22, 32]. Despite inherent oversimplifications, it is possible to keep some degree of physical representativeness by adopting the hypothesis of a fully developed flow [14]. However, even in such a setting it is necessary to solve a nonstandard *inverse problem* in order to evaluate velocity and pressure, from an assigned flux. As a further caveat, we observe that we deliberately confine our attention to basic fluid mechanics effects associated with deviation from an idealized circular cross section. Hence, despite our interest in the considered biological flows, we do not address near-wall conditions (e.g., wall shear stress and temporal/spatial derivatives) and transport phenomena (e.g., mixing and residence times), which play a role in physiological investigations.

In light of the above observations, we consider fully developed flows of an incompressible Newtonian fluid in a straight cylinder with elliptical cross section, either simply connected or not. These assumptions permit us to address a simplified linear problem, and our approach aims at obtaining a benchmark solution for the inverse problem. More precisely, by virtue of the fully developed flow hypothesis, we provide a numerical strategy which is substantially grounded on analytical relations, while being more amenable to implementation than previous approaches proposed in literature. Hence, while laying no claims of generality, since we do not address complex/deformable geometries and/or rheological effects, the method we propose is credited to hold some value for obtaining at least an approximation to real flows, with a contained computational effort. Furthermore, the same strategy can be used to produce improved boundary data for more ambitious numerical approaches based on realistic data. The numerical study of this inverse problem also seems completely new and original.

We consider an incompressible Newtonian fluid, with constant density normalized to unity, in a semi-infinite straight pipe $P = E \times \mathbf{R}^+ \subset \mathbf{R}^3$, where $E \subset \mathbf{R}^2$ will be either an ellipse or an elliptical annulus. In a reference frame with z directed along the pipe axis and $x = (x_1, x_2)$ belonging to an orthogonal plane, the Navier–Stokes equations read

$$\begin{aligned} \partial_t \vec{u} + (\vec{u} \cdot \nabla)\, \vec{u} - \nu \Delta \vec{u} + \nabla p = 0, &\qquad (x, z) \in E \times \mathbf{R}^+,\ t \in \mathbf{R}^+, \\ \nabla \cdot \vec{u} = 0, &\qquad (x, z) \in E \times \mathbf{R}^+,\ t \in \mathbf{R}^+, \\ \vec{u} = 0, &\qquad (x, z) \in \partial E \times \mathbf{R}^+,\ t \in \mathbf{R}^+, \end{aligned}$$

where $\vec{u}(t, x, z)$ and $p(t, x, z)$ respectively denote velocity and pressure and $\nu > 0$ represents kinematic viscosity. We look for fully developed solutions (also named Poiseuille-type solutions),

$$\vec{u}(t, x, z) = (0, 0, w(t, x)) \qquad \text{and} \qquad p(t, x, z) = -\lambda(t, x, z) + p_0(t),$$

where $p_0(t)$ is an arbitrary function of time. Moreover, the flux condition $\int_E w(t, x)\, dx = f(t)$ is assumed for some given scalar function $f(t)$. The Poiseuille-type *ansatz* implies that the convective term cancels out and that pressure is $p(t, z) = -\lambda(t)\, z$. Finally, the dependence of w on the space variables x_1 and x_2 allows us to consider a

problem reduced to the cross section E: Given $f(t)$, find $(w(t,x), \lambda(t))$ such that

$$\begin{cases} \partial_t w(t,x) - \nu \Delta_x w(t,x) = \lambda(t), & x \in E,\ t \in \mathbf{R}^+, \\ w(t,x) = 0, & x \in \partial E,\ t \in \mathbf{R}^+, \\ \int_E w(t,x)\, dx = f(t), & t \in \mathbf{R}^+, \end{cases} \tag{1.1}$$

where Δ_x denotes the Laplacian with respect to the variables x_1 and x_2. This inverse problem is linked to one of the nowadays classical Leray's problems. Results of existence and uniqueness for (1.1) are known in cylindrical pipes with very general cross sections, under reasonable technical assumptions; see [4, 6]. Conversely, explicit and/or practical computation of the solutions seems hardly obtainable for general cross sections, so that we restrict to an ellipse or to the annulus between confocal ellipses.

The relevance of the cross section shape deserves some discussion: For a circular cross section, by writing the Laplace operator in cylindrical coordinates, one can obtain an explicit analytical solution for the direct problem in terms of Bessel functions; cf. [31, 38] and section 3. Recently we derived in [5] an analytical solution to the inverse problem involving regularized confluent hypergeometric functions. For an elliptical cross section, in spite of the apparent similarity to the circular case, the situation drastically changes: By using Mathieu functions [23], an explicit solution can be obtained only for the stationary problem, while it is necessary to resort to numerical computations already when addressing the direct time-dependent problem [16, 27, 36, 37]. Some numerical approaches tackling the inverse problem have been recently proposed [14], still by invoking the Mathieu functions and the determination of the Laplacian's eigenvalues in an elliptical domain. This is not a trivial task since severe instabilities can arise in managing the Mathieu functions, especially when the ellipticity parameter $\varepsilon = \beta/\alpha$ (the ratio between the lengths of the minor and major semiaxes) is small [16], and their computation has been assessed as a critical issue in the numerical procedure; see [14].

In light of these points, we propose an alternative numerical approach which indirectly addresses the Mathieu problem and which does not suffer from the aforementioned limitations. Some numerical simulations are also reported, based on flow rates coming from measurements of human blood flow in the internal carotid artery and CSF flow in the upper cervical region of the human spine. The results support the effective usability of our formulation, which is also capable of dealing with very small ε.

2. Stationary problem. Despite being classical, the stationary solution in the circular and elliptical cross sections is rederived in a way that is functional to the subsequent treatment. Such a stationary problem is formulated as a Poisson problem: Given the flux $f \in \mathbf{R}$, find $(w(x), \lambda)$ such that

$$\begin{cases} -\nu \Delta_x w(x) = \lambda, & x \in E, \\ w(x) = 0, & x \in \partial E, \\ \int_E w(x)\, dx = f. \end{cases} \tag{2.1}$$

2.1. Stationary flow in a circular cross section. Hagen and Poiseuille first derived the solution in a circular domain by separation of variables; their solution is still used as a benchmark flow, e.g., for turbulence studies or for recent biomedical applications such as magnetic particle targeting. This is mainly due to the fact that

Poiseuille flow represents one of the few examples of exact solutions of fluid equations with Dirichlet boundary conditions.

2.1.1. Flow in the circle. Let $E = \{(x_1, x_2) \in \mathbf{R}^2 : \ |x| < R\}$ be a circle centered at the origin, with radius $R > 0$, where $|x| = \sqrt{x_1^2 + x_2^2}$. The solution to (2.1) is easily obtained as follows:

$$w(x) = \frac{2f}{\pi R^2}\left(1 - \frac{|x|^2}{R^2}\right). \tag{2.2}$$

2.1.2. Flow in the circular annulus. Let $E = \{(x_1, x_2) \in \mathbf{R}^2 : \ R_1 < |x| < R_2\}$ be a circular annulus delimited by radii $R_1 < R_2$. In this case the solution of the Poisson problem (2.1) is

$$w(x) = \frac{2f}{\pi\, R_2^2} \frac{\left(1 - \frac{|x|^2}{R_2^2}\right) - \left(1 - \frac{R_1^2}{R_2^2}\right) \frac{\log\left(\frac{|x|}{R_2}\right)}{\log\left(\frac{R_1}{R_2}\right)}}{\left(1 - \frac{R_1^4}{R_2^4}\right) + \left(1 - \frac{R_1^2}{R_2^2}\right)^2 \frac{1}{\log\left(\frac{R_1}{R_2}\right)}}. \tag{2.3}$$

Notice the limiting behavior of (2.3) for $R_2 = R$ and $R_1 \to 0$.

2.2. Stationary flow in an elliptical cross section. Original solutions for this problem appeared in the pioneering works of Verma [37, 36], yet a previous work by Khamrui was cited therein. Thanks to their particularly simple expression of the external force, it is still possible to obtain an analytical solution by using Mathieu functions (while numerics in presence of more general external forces is the subject of ongoing research; see [20]). We introduce a derivation which will also be useful for handling the time-dependent case later on.

2.2.1. Flow in the ellipse. Let $E = \{(x_1, x_2) \in \mathbf{R}^2 : x_1^2/\alpha^2 + x_2^2/\beta^2 < 1\}$ denote an ellipse, where $\alpha = a\cosh(b)$ and $\beta = a\sinh(b)$ respectively indicate the length of the major (x_1-direction) and minor (x_2-direction) semiaxes, while $2a = 2\sqrt{\alpha^2 - \beta^2}$ represents the interfocal distance. The two equalities defining b, namely $\cosh^{-1}(\alpha/a) = b = \sinh^{-1}(\beta/a)$, imply $\log\left(\alpha/a + \sqrt{\alpha^2 - a^2}/a\right) = \log(\beta/a + \sqrt{\beta^2 + a^2}/a)$, from which we get $b = \log\left((\alpha + \beta)/a\right)$. Then, to construct the solution we introduce the natural change of variables

$$x_1 = a\cosh(\eta)\cos(\theta) \qquad \text{and} \qquad x_2 = a\sinh(\eta)\sin(\theta), \tag{2.4}$$

with Jacobian

$$J(\eta, \theta) = a^2\left[\sinh^2(\eta) + \sin^2(\theta)\right] = \frac{a^2}{2}\left[-\frac{e^{-2i\theta}}{2} + \cosh(2\eta) - \frac{e^{2i\theta}}{2}\right]. \tag{2.5}$$

By employing this change of variables we reduce to a problem in the rectangular domain:

$$E' = \{(\eta, \theta) \in \mathbf{R}^2 : \ 0 < \eta < b \quad \text{and} \quad 0 \le \theta < 2\pi\}. \tag{2.6}$$

The Laplace operator is still separable in these coordinates, and the Poisson equation (2.1) becomes

$$\begin{cases} -\dfrac{\nu}{J(\eta,\theta)}\left(\dfrac{\partial^2 u}{\partial\eta^2}+\dfrac{\partial^2 u}{\partial\theta^2}\right)=\lambda, & (\eta,\theta)\in E', \\ \quad u \text{ is } 2\pi\text{-periodic in } \theta & \\ \qquad\qquad u(b,\theta)=0, & \theta\in[0,2\pi[, \\ \displaystyle\int_{E'} u(\eta,\theta)\,J(\eta,\theta)\,d\eta\,d\theta=f, & \end{cases}$$

where $u(\eta,\theta)$ simply represents $w(x)$ in the new variables (notice also that $J>0$ for $\eta>0$). Due to θ-periodicity, the solution can be written as a Fourier series ($\widehat{\cdot}$ denotes a complex Fourier coefficient):

$$u(\eta,\theta)=\sum_{n\in\mathbf{Z}}\widehat{u}_n(\eta)\,e^{in\theta}, \qquad \text{where} \qquad \widehat{u}_n(\eta)=\frac{1}{2\pi}\int_0^{2\pi} u(\eta,\theta)\,e^{-in\theta}.$$

By linearity, we temporarily assume $\lambda=1$, and we recast the problem as follows (not assigning the flux): Find u, 2π-periodic in θ, such that

$$\begin{cases} -\nu\Big(\dfrac{\partial^2 u}{\partial\eta^2}+\dfrac{\partial^2 u}{\partial\theta^2}\Big)=J(\eta,\theta), & (\eta,\theta)\in E', \\ \qquad u(b,\theta)=0, & \theta\in[0,2\pi[. \end{cases}$$

Employing Fourier variables, we also require $\widehat{u}_{-n}=\overline{\widehat{u}_n}$ to have a real-valued velocity ($\bar{\cdot}$ denotes complex conjugacy). Denoting by $\Re$ and $\Im$ the real and imaginary parts, respectively, it follows that $\Im(\widehat{u}_0)=0$. Then, by using the axes reflection symmetries of the solution, it follows that $\widehat{u}_n=0$ for n odd. Moreover, to have a smooth solution at $\eta=0$, we impose $\partial_\eta u(0,\theta)=0$. By observing that J possesses only three nonzero modes (associated with $n=-2,0,2$), we obtain the following identity corresponding to a system of three complex ordinary differential equations, where "prime" $(\cdot\,')$ denotes the derivative with respect to η:

$$-\nu\sum_{n=-2,0,2}\left[\widehat{u}_n''(\eta)-n^2\widehat{u}_n(\eta)\right]e^{in\theta}=\frac{a^2}{2}\left[-\frac{e^{-2i\theta}}{2}+\cosh(2\eta)-\frac{e^{2i\theta}}{2}\right].$$

Then, enforcing conditions at $\eta=0,b$, we must solve the following boundary value problems in $[0,b]$:

$$\begin{cases} \widehat{u}_{\pm2}''(\eta)-4\widehat{u}_{\pm2}=\dfrac{a^2}{4\nu}, \\ \widehat{u}_{\pm2}(b)=\Re(\widehat{u}_{\pm2}'(0))=\Im(\widehat{u}_{\pm2}(0))=0, \end{cases} \qquad \text{and} \qquad \begin{cases} \widehat{u}_0''(\eta)=-\dfrac{a^2}{2\nu}\cosh(2\eta), \\ \widehat{u}_0(b)=\widehat{u}_0'(0)=0. \end{cases}$$

By explicitly solving these *uncoupled* linear differential equations, we get

$$\widehat{u}_0(\eta)=-\frac{a^2}{8\nu}\left(\cosh(2\eta)-\cosh(2b)\right), \qquad \widehat{u}_{\pm2}(\eta)=-\frac{a^2}{16\nu}\frac{1+e^{4b}-e^{2b-2\eta}-e^{2b+2\eta}}{1+e^{4b}}.$$

Then, after some algebraic manipulations, the solution to the Poisson problem with $\lambda=1$ is

$$u(\eta,\theta)=\frac{a^2}{8\nu}\left(\cosh(2b)-\cos(2\theta)\right)\left(\cosh(2b)-\cosh(2\eta)\right)\operatorname{sech}(2b),$$

with corresponding flux

$$\int_{E'} u(\eta,\theta)\, J(\eta,\theta)\, d\eta\, d\theta = a^2 \int_0^b \int_0^{2\pi} u(\eta,\theta)\, [\sinh^2(\eta) + \sin^2(\theta)]\, d\theta\, d\eta$$
$$= \frac{\pi a^4}{32\nu} \sinh^2(2b)\, \tanh(2b).$$

The solution to the original problem (2.1) with assigned flux f is finally obtained as $(\lambda u(\eta,\theta), \lambda)$, where

$$\lambda = f\, \frac{32\nu}{\pi a^4} \left[\sinh^2(2b)\, \tanh(2b)\right]^{-1}.$$

Finally, by mapping back to Cartesian coordinates, we get

$$w(x_1,x_2) = \frac{2f}{\pi\alpha\beta}\left[1 - \frac{x_1^2}{\alpha^2} - \frac{x_2^2}{\beta^2}\right]. \tag{2.7}$$

It is interesting to note how (2.7) derives from Poiseuille solution (2.2) by an anisotropic scaling of the variables. Thus, the elegant expression (2.7), which appears in [16] but is missing in many related works, could have been obtained through simpler derivations. We decided to follow this path, which will be used later on for the solution of the time-dependent problem, since a simple scaling of the variables is not suitable in that case. In fact, it should be noticed how—despite separation of variables—elliptical domains per se create a new situation already in the stationary case: Contrarily to the solution in the circle, even in presence of a constant force there appear three active modes. Such a difference persists and is somehow magnified in the time-dependent case; see section 3.

2.2.2. Flow in the elliptical annulus. We consider now the motion between two confocal ellipses; only in this setting, the annulus is still mapped in a rectangular domain by (2.4). More precisely, given the outer ellipse semiaxes α_2, β_2, the interfocal semidistance is $a = \sqrt{\alpha_2^2 - \beta_2^2}$. Once assigned the minor semiaxis $\beta_1 < \beta_2$ of the inner ellipse, necessarily $\alpha_1 = \sqrt{\alpha_2^2 - \beta_2^2 + \beta_1^2}$. Then, the annulus between the two ellipses is mapped into the rectangle $E' = \{(\eta,\theta) \in \mathbf{R}^2 :\ b_1 < \eta < b_2 \text{ and } 0 \le \theta < 2\pi\}$, where $b_i = \log((\alpha_i + \beta_i)/a)$. Vanishing Dirichlet boundary conditions are imposed at $\eta = b_1$, b_2 and, to have real-valued velocities, we impose $\widehat{u}_{-n} = \overline{\widehat{u}_n}$, ending up with the following auxiliary boundary value problems with $\lambda = 1$:

$$\begin{cases} \widehat{u}''_{\pm 2}(\eta) - 4\widehat{u}_{\pm 2} = \dfrac{a^2}{4\nu}, \\ \widehat{u}_{\pm 2}(b_1) = \widehat{u}_{\pm 2}(b_2) = 0, \end{cases} \qquad \text{and} \qquad \begin{cases} \widehat{u}''_0(\eta) = -\dfrac{a^2}{2\nu}\cosh(2\eta), \\ \widehat{u}_0(b_1) = \widehat{u}_0(b_2) = 0. \end{cases}$$

By explicit calculations, the solutions read

$$\widehat{u}_0(\eta) = \frac{a^2}{8\nu}\left[\frac{(\eta - b_1)\cosh(2b_2) - (\eta - b_2)\cosh(2b_1)}{(b_2 - b_1)} - \cosh(2\eta)\right],$$
$$\widehat{u}_{\pm 2}(\eta) = \frac{a^2}{16\nu}\left[\frac{e^{2(\eta - b_2)} - e^{-2(\eta - b_2)} - e^{2(\eta - b_1)} + e^{-2(\eta - b_1)}}{e^{2(b_1 - b_2)} - e^{-2(b_1 - b_2)}} - 1\right],$$

so that the following stationary solution for the auxiliary problem is obtained (cf. [36]):

$$u(\eta,\theta) = \frac{a^2}{8\nu}\left[\frac{(\eta - b_1)\cosh(2b_2) - (\eta - b_2)\cosh(2b_1)}{(b_2 - b_1)}\right.$$
$$\left. + \frac{\sinh(2(\eta - b_1)) - \sinh(2(\eta - b_2))}{\sinh(b_2 - b_1)}\cos(2\theta) - (\cosh(2\eta) + \cos(2\theta))\right].$$

By reasoning as in section 2.2.1, the solution to (2.1) is given by $(\lambda u(\eta,\theta),\lambda)$, with (cf. [14])

$$\lambda = f\,\frac{16\nu}{\pi a^4}\left[\frac{(\sinh(4b_2)-\sinh(4b_1))}{4} - \frac{(\cosh(2b_2)-\cosh(2b_1))^2}{2(b_2-b_1)} - \frac{\cosh(2(b_2-b_1))-1}{\sinh(2(b_2-b_1))}\right]^{-1}.$$

It is worth remarking that the solution in the ellipse cannot be obtained as a limit case from the annulus, due to the constraint of confocality. Indeed, for $b_1 \to 0$ the inner boundary of the annulus (with Dirichlet condition) degenerates to the interfocal segment, and one obtains the flow field in an ellipse which also contains a plate.

3. Time-dependent problem. We now address the time-periodic elliptical case, by proposing a novel numerical method for its solution. We first recall the Womersley solution as well as that of the inverse problem in the circular case, to keep some degree of symmetry with section 2. We then address the elliptical case, and we accurately report the solution method for the simply connected elliptical cross section, while full details for the elliptical annulus between two confocal ellipses are skipped, since they can easily be derived by the interested reader. We just remark that the proposed method does not apply to nonconfocal ellipses, because in the general case separation of variables is not viable.

3.1. Flow in the circle: Direct and inverse problem. Let us preliminarily introduce the following T-periodic functions:

$$\begin{aligned} \lambda(t) &= \sum_{m\in\mathbf{Z}} \widehat{\lambda}_m e^{i\omega_m t}, \quad f(t) = \sum_{m\in\mathbf{Z}} \widehat{f}_m e^{i\omega_m t}, \\ w(x,t) &= \sum_{m\in\mathbf{Z}} \widehat{w}_m(x)\, e^{i\omega_m t}, \quad \omega_m = \frac{2\pi m}{T}. \end{aligned} \tag{3.1}$$

We then recall that the direct problem $\partial_t w(t,x) - \nu\Delta_x w(t,x) = \lambda(t)$, with assigned $\lambda(t) = \widehat{\lambda}_m\, e^{i\omega_m t}$ (a single Fourier mode) has been considered by Womersley [38]. In cylindrical variables it becomes $\widehat{w}_m''(r) + \widehat{w}_m'(r)/r - i\,\omega_m\,\widehat{w}_m(r)/\nu = -\widehat{\lambda}_m/\nu$, with $r = \sqrt{x_1^2+x_2^2}$. The explicit solution can be expressed through the zeroth order Bessel functions J_0, as follows:

$$w(r,t) = \widehat{w}_m(r)\, e^{i\omega_m t} = \left(1 - \frac{J_0\left((-1)^{3/4}\,\mathrm{Wo}_{r,m}\right)}{J_0\left((-1)^{3/4}\,\mathrm{Wo}_{R,m}\right)}\right)\,\frac{\widehat{\lambda}_m}{i\,\omega_m}\, e^{i\omega_m t}, \tag{3.2}$$

where $\mathrm{Wo}_{r,m} = r\,\sqrt{\frac{\omega_m}{\nu}}$ is a nondimensional parameter, with a notation which slightly generalizes that introduced by Womersley. Given w, one can evaluate the flux. Conversely, starting from a given flux $\widehat{f}_m\, e^{i\omega_m t}$, the explicit map between $\widehat{w}_m$ and $\widehat{f}_m$ has been recently obtained in [5]:

$$\begin{aligned} \widehat{f}_m &= \pi R^2\,\left(1 - \frac{{}_0\tilde{F}_1\left(;2;i\,\mathrm{Wo}_{R,m}^2/4\right)}{{}_0\tilde{F}_1\left(;1;i\,\mathrm{Wo}_{R,m}^2/4\right)}\right)\,\frac{\widehat{\lambda}_m}{i\omega_m}, \\ \widehat{w}_m(r) &= \left(1 - \frac{J_0\left((-1)^{3/4}\,\mathrm{Wo}_{r,m}\right)}{J_0\left((-1)^{3/4}\,\mathrm{Wo}_{R,m}\right)}\right)\,\frac{\widehat{\lambda}_m}{i\omega_m}, \end{aligned}$$

where ${}_0\tilde{F}_1(;\cdot;\cdot)$ denotes the regularized confluent hypergeometric function. Since the problem is linear, superposition can be invoked and, under the assumptions on f in [4], the series $\sum_{m\in\mathbf{Z}} \widehat{w}_m(r)\, e^{i\omega_m t}$ converges to the solution of (1.1).

3.2. Flow in the ellipse: The auxiliary direct problem. The explicit solution for the direct problem in an elliptical vessel was originally derived by Verma [37], following the same approach of Womersley, although some details were missing. In particular, given a single harmonic pressure gradient $\lambda = e^{i\omega_m t}$, with $m \in \mathbf{Z}$, the solution in elliptical coordinates is

$$u(\eta,\theta) = \sum_{n=0}^{\infty} C_{2n}\; Ce_{2n}(\eta,-q)\, ce_{2n}(\theta,-q) \qquad \text{with } q = \frac{i\, a^2\, \omega_m}{4\,\nu}, \tag{3.3}$$

where Ce_{2n} and ce_{2n} are the ordinary and modified Mathieu functions [23] while C_{2n} represent suitable constants, determined from the no-slip boundary condition. Mathieu functions were introduced in the 19th century to study the vibration of an elliptical membrane, but they still deserve attention from a computational viewpoint, since their evaluation is prone to severe numerical instabilities [33]. Moreover, in order to get a 2π-periodic solution in θ through the Mathieu functions, one needs to evaluate the eigenvalues of the Laplacian: This involves infinite tridiagonal matrices and is very expensive. Furthermore, practical limitations on the ellipticity parameter ε arise when directly using these special functions, and numerical instabilities are reported for $\varepsilon < 0.3$ in [16]. In light of these points, the quest for robust numerical methods to efficiently compute the Mathieu functions is still an open issue. A stepwise procedure has been proposed in [14], in correspondence to large complex arguments typically associated with viscous flows, with a proper blend of backward and forward recurrence techniques, aimed at enhancing convergence.

To circumvent the aforementioned limitations, we propose a novel numerical strategy, in the spirit of Fourier analysis, which involves the Mathieu functions only in an *indirect way*, and we extend methods from [20] for the stationary case. Our approach is based on Fourier analysis in the variables θ and t, while η is kept in the physical space. With the change of variables (2.4), we recast the problem as

$$u_t(t,\eta,\theta)\, J(\eta,\theta) - \nu\left(\frac{\partial^2 u(t,\eta,\theta)}{\partial\eta^2} + \frac{\partial^2 u(t,\eta,\theta)}{\partial\theta^2}\right) = J(\eta,\theta)\,\lambda(t). \tag{3.4}$$

Since we look for T-time-periodic and 2π-θ-periodic solutions, we make the ansatz

$$u(t,\eta,\theta) = \sum_{m,n\in\mathbf{Z}} \widehat{u}_{m,n}(\eta)\, e^{in\theta} e^{i\omega_m t}, \tag{3.5}$$

and to have real-valued solutions we impose $\widehat{\lambda}_{-m} = \overline{\widehat{\lambda}_m}$, $\widehat{f}_{-m} = \overline{\widehat{f}_m}$, and $\widehat{u}_{-m,-n} = \overline{\widehat{u}_{m,n}}$. (The latter relation implies, in particular, $\Im(\widehat{u}_{0,0}(\eta)) = 0$.)

We start by addressing a *direct* problem, with *given* pressure gradient. Within this section, to stress the fact that we temporarily turn our attention to a direct problem, we denote the pressure gradient by $\sigma(t) = \sum_{m\in\mathbf{Z}} \widehat{\sigma}_m e^{i\omega_m t}$. By plugging (3.5) into (3.4), we get: Solve, for each $m \in \mathbf{Z}$,

$$\begin{cases} \displaystyle\sum_{n\in\mathbf{Z}} i\,\omega_m \widehat{u}_{m,n}(\eta)\, e^{in\theta} J(\eta,\theta) - \nu\big(\widehat{u}''_{m,n}(\eta) - n^2\widehat{u}_{m,n}(\eta)\big)\, e^{in\theta} = J(\eta,\theta)\,\widehat{\sigma}_m, \\ \qquad\qquad\qquad\qquad\qquad\qquad\qquad\qquad \widehat{u}_{m,n}(b) = 0, \qquad n \in \mathbf{Z}, \end{cases} \tag{3.6}$$

with $(\eta, \theta) \in E'$ and E' defined as in (2.6). System (3.6) can be simplified by invoking symmetry: Velocity must be unchanged by the transformations $\theta \mapsto -\theta$ and $\theta \mapsto \pi - \theta$, i.e., by reflection over the ellipse axes of symmetry. By also recalling the conditions on conjugacy, this provides

$$\begin{gathered}\widehat{u}_{m,n} = 0 \text{ for } n \text{ odd} \qquad \text{and} \\ \widehat{u}_{m,-n} = \widehat{u}_{m,n},\ \widehat{u}_{-m,n} = \overline{\widehat{u}_{m,-n}} = \overline{\widehat{u}_{m,n}} \quad \text{for } n \text{ even, } m \in \mathbf{Z}.\end{gathered} \tag{3.7}$$

Hence, we need to evaluate only the Fourier modes $\widehat{u}_{m,n}$, with $0 < n, m \in \mathbf{Z}$, and n even. This reduces by a factor eight the computational burden. By plugging (2.5) into (3.6) and by equating the corresponding even n-modes (at fixed m), we obtain the following infinite family of ordinary differential equations:

$$\begin{aligned}
&\widehat{u}''_{m,0} - \left[\frac{i\,\mathrm{Wo}^2_{a,m}}{2}\cosh(2\eta)\right]\widehat{u}_{m,0} + \frac{i\,\mathrm{Wo}^2_{a,m}}{2}\,\widehat{u}_{m,2} = -\tfrac{a^2}{2\nu}\cosh(2\eta)\,\widehat{\sigma}_m,\\
&\widehat{u}''_{m,2} - \left[2^2 + \frac{i\,\mathrm{Wo}^2_{a,m}}{2}\cosh(2\eta)\right]\widehat{u}_{m,2} + \frac{i\,\mathrm{Wo}^2_{a,m}}{4}\left(\widehat{u}_{m,4} + \widehat{u}_{m,0}\right) = \tfrac{a^2}{4\nu}\,\widehat{\sigma}_m,\\
&\widehat{u}''_{m,4} - \left[4^2 + \frac{i\,\mathrm{Wo}^2_{a,m}}{2}\cosh(2\eta)\right]\widehat{u}_{m,4} + \frac{i\,\mathrm{Wo}^2_{a,m}}{4}\left(\widehat{u}_{m,6} + \widehat{u}_{m,2}\right) = 0,\\
&\qquad\vdots \qquad\qquad \vdots \quad \vdots\\
&\widehat{u}''_{m,2n} - \left[(2n)^2 + \frac{i\,\mathrm{Wo}^2_{a,m}}{2}\cosh(2\eta)\right]\widehat{u}_{m,2n}\\
&\qquad + \frac{i\,\mathrm{Wo}^2_{a,m}}{4}\left(\widehat{u}_{m,2n+2} + \widehat{u}_{m,2n-2}\right) = 0,\\
&\qquad\vdots \qquad\qquad \vdots \quad \vdots
\end{aligned} \tag{3.8}$$

where, for brevity, we use $\widehat{u}_{m,n}$ in place of $\widehat{u}_{m,n}(\eta)$ and $\mathrm{Wo}_{a,m}$ is a generalized Womersley number based on the interfocal semidistance a, defined as in (3.2) and consistent with [14, 16]; cf. (3.3) with $q = i\mathrm{Wo}^2_{a,m}/4$. Furthermore, to have a well-posed system we assign another condition at the singular point $\eta = 0$ of the change of coordinates, enforcing symmetry for the velocity-profile (cf. [16, eq. (9)]) by $\partial_\eta u(0, \theta, t) = 0$.

Equations (3.8) are an infinite system of nonhomogeneous Mathieu equations. In order to get a computable system, one main idea is to use an approximation with a finite-dimensional system. However, this cannot be achieved by simply neglecting all equations which involve modes $\widehat{u}_{m,n}$ for large enough $|n|$, since there is an infinite coupling (the nth mode is coupled with the two closest modulo 2).

Provided that $|\widehat{f}_m|$ decays fast enough as $|m| \to +\infty$ (and this is more than reasonable for realistic flows; see also section 4), the coefficients $\widehat{u}_{m,n}$ are asymptotically small, since they belong to a convergent Fourier series [4, 6, 12]. In practical computations, we assume that $|\widehat{f}_m|$ is negligible for $|m| > M$ for some $M \in \mathbf{N}$. The index M affects the quality of the truncated flow rate, and its choice is also determined by measurement issues beyond the present scope. Yet we assume that M is chosen large enough to accurately reproduce the experimental flow, while also avoiding truncation artifacts. A cut-off index $N \in \mathbf{N}$ is then chosen such that, by neglecting $\widehat{u}_{m,n}$ for all $n \in \mathbf{Z}$ with $|n| > 2N$, it does not significantly affect the solution. Obviously, it must be $N \geq 2$ to keep at least the first equations having nonzero right-hand side. This implies that we can drop off $\widehat{u}_{m,2N+2}$ in the differential equation satisfied by $\widehat{u}_{m,2N}$, and solve only the equations for $\widehat{u}_{m,n}$ with $n = 0, 2, \ldots, 2N$. In this way, for each

considered m, we end up with a closed tridiagonal system of linear ordinary differential equations, a differential counterpart of the tridiagonal matrix obtained when approximating the eigenvalues of the Mathieu functions; see [1, 14].

By linearity, it is convenient to assume $\widehat{\sigma}_m = 1$, and we denote the unknown by $\widehat{v}_{m,n}$ to stress that we are approximating $\widehat{u}_{m,n}$ by truncation. Then, for each $m \in \{0, \ldots, M\}$ we have to solve

(3.9)
$$\begin{cases} \widehat{v}''_{m,0} - \left[\frac{i\,\mathrm{Wo}^2_{a,m}}{2}\cosh(2\eta)\right]\widehat{v}_{m,0} + \frac{i\,\mathrm{Wo}^2_{a,m}}{2}\widehat{v}_{m,2} = -\frac{a^2}{2\nu}\cosh(2\eta), \\ \widehat{v}''_{m,2} - \left[2^2 + \frac{i\,\mathrm{Wo}^2_{a,m}}{2}\cosh(2\eta)\right]\widehat{v}_{m,2} + \frac{i\,\mathrm{Wo}^2_{a,m}}{4}(\widehat{v}_{m,4} + \widehat{v}_{m,0}) = \frac{a^2}{4\nu}, \\ \widehat{v}''_{m,4} - \left[4^2 + \frac{i\,\mathrm{Wo}^2_{a,m}}{2}\cosh(2\eta)\right]\widehat{v}_{m,4} + \frac{i\,\mathrm{Wo}^2_{a,m}}{4}(\widehat{v}_{m,6} + \widehat{v}_{m,2}) = 0, \\ \qquad\vdots \qquad\qquad = \vdots \\ \widehat{v}''_{m,2n} - \left[(2n)^2 + \frac{i\,\mathrm{Wo}^2_{a,m}}{2}\cosh(2\eta)\right]\widehat{v}_{m,2n} + \frac{i\,\mathrm{Wo}^2_{a,m}}{4}(\widehat{v}_{m,2n+2} + \widehat{v}_{m,2n-2}) = 0, \\ \qquad\vdots \qquad\qquad = \vdots \\ \widehat{v}''_{m,2N-2} - \left[(2N-2)^2 + \frac{i\,\mathrm{Wo}^2_{a,m}}{2}\cosh(2\eta)\right]\widehat{v}_{m,2N-2} \\ \qquad + \frac{i\,\mathrm{Wo}^2_{a,m}}{4}(\widehat{v}_{m,2N} + \widehat{v}_{m,2N-4}) = 0, \\ \widehat{v}''_{m,2N} - \left[(2N)^2 + \frac{i\,\mathrm{Wo}^2_{a,m}}{2}\cosh(2\eta)\right]\widehat{v}_{m,2N} + \frac{i\,\mathrm{Wo}^2_{a,m}}{4}(\widehat{v}_{m,2N-2}) = 0, \\ \widehat{v}_{m,n}(b) = 0, \qquad n = 0, 2, \ldots, 2N, \\ \widehat{v}'_{m,n}(0) = 0, \qquad n = 0, 2, \ldots, 2N. \end{cases}$$

It should be noted that, once the fluid viscosity and the semiaxes α and β are fixed, the solution of (3.9) is affected only by the cut-off index N. We stress this point by introducing the notation $\widehat{v}^{(2N)}_{m,n}$, and we denote by $N^\star$ a truncation index to be chosen large enough to get a proper approximation. Two assets can be introduced for the purpose: (i) accuracy, since magnitude of the cut modes must be negligible compared to that of the kept ones; (ii) independence from N, since truncation must affect the kept modes in only a negligible way. Recalling that the amplitude of high frequencies is expected to be smaller than that of low ones, the accuracy asset can be formulated by introducing the following nondimensional quantity:

$$\mu(m, N) = \frac{\|\widehat{v}^{(2N)}_{m,2N}\|_\infty}{\|\widehat{v}^{(2N)}_{m,0}\|_\infty}, \tag{3.10}$$

where $\|\widehat{v}\|_\infty = \max_{0 \le \eta \le b \in E'_\eta} |\widehat{v}(\eta)|$ and the $n = 0$ mode is used to get a reference value. (Such a reference was used for the numerical tests in section 4, turning out to be nonvanishing; alternative choices can be introduced by exploiting larger values of n.) Once we have chosen a threshold $\bar{\mu}$, let us define $N^\star_{\bar{\mu}}$ as the smallest $N \in \mathbf{N}$ such that $\mu(m, N) \le \bar{\mu}$ for all $m \in \{0, \ldots, M\}$. Hence, by choosing $N \ge N^\star_{\bar{\mu}}$, we are guaranteed that truncation cuts only negligible n-modes for all relevant values of m. As regards independence from N, the following nondimensional quantity is introduced:

$$s(m, N) = \max_{n \in \mathcal{N}} \frac{\|\widehat{v}^{(2N)}_{m,n} - \widehat{v}^{(2N+2)}_{m,n}\|_\infty}{\|\widehat{v}^{(2N)}_{m,0}\|_\infty}, \tag{3.11}$$

where $\mathcal{N} = \{0, 2, \dots, 2N-2\}$ (the index $2N$ is not considered, for obvious reasons). Once a threshold $\bar{s}$ has been chosen, $N^\star_{\bar{s}}$ is the smallest $N \in \mathbf{N}$ such that $s(m, N) \le \bar{s}$ for all considered m. Hence, by choosing $N \ge N^\star_{\bar{s}}$, we are guaranteed that truncation only negligibly affects the kept n-modes for all relevant values of m. Finally, we define $N^\star = \max\big(N^\star_{\bar{\mu}}, N^\star_{\bar{s}}\big)$.

3.3. Flow in the ellipse: The inverse problem. We propose here a method, alternative to that recently provided in [14], which is based on the Fourier approach introduced in section 3.2. Thanks to linearity, we simply need to link the Fourier coefficients of the flow rate with those of the pressure gradient. The flow rate associated with the solution coming from ansatz (3.5) is

$$f(t) = \sum_{m\in\mathbf{Z}} \widehat{f}_m\, e^{i\omega_m t} = \sum_{m\in\mathbf{Z}} \left[\sum_{n\in\mathbf{Z}} \int_0^b \widehat{u}_{m,n}(\eta) \left(\int_0^{2\pi} e^{in\theta}\, J(\eta,\theta)\, d\theta \right) d\eta \right] e^{i\omega_m t}.$$

Then, substituting J from (2.5), by explicit calculations we get

$$\frac{1}{a^2} \int_0^{2\pi} e^{in\theta}\, J(\eta,\theta)\, d\theta = \begin{cases} -\pi/2, & n = \pm 2, \\ \pi \cosh(2\eta), & n = 0, \\ 0, & n \in \mathbf{Z}\backslash\{0, \pm 2\}, \end{cases}$$

so that the following relation can be easily obtained for each $m \in \mathbf{Z}$:

$$\widehat{f}_m = \frac{a^2\pi}{2} \int_0^b \Big(-\widehat{u}_{m,-2}(\eta) + 2\cosh(2\eta)\, \widehat{u}_{m,0}(\eta) - \widehat{u}_{m,2}(\eta) \Big)\, d\eta. \tag{3.12}$$

Clearly, without an explicit knowledge of $\widehat{u}_{m,n}(\eta)$ it is not possible to evaluate the flux by means of (3.12). Nevertheless, by the approximate solution $\widehat{v}_{m,n}$ from section 3.2, it is straightforward to exploit (3.12) in order to approximate the Fourier coefficients $\widehat{\lambda}_m$ in terms of $\widehat{f}_m$ as follows:

$$\widehat{\lambda}_m \cong \widehat{f}_m \frac{1}{\pi a^2} \left[\int_0^b \big(\cosh(2\eta)\, \widehat{v}_{m,0}(\eta) - \widehat{v}_{m,2}(\eta) \big)\, d\eta \right]^{-1}, \qquad m \in \mathbf{N} \cup \{0\}. \tag{3.13}$$

The bracketed quantity must be nonvanishing for such an expression to be meaningful. For the *exact* solution $\widehat{u}_{m,n}$ the map between $\widehat{f}_m$ and $\widehat{\lambda}_m$ is one-to-one, implying a nonvanishing denominator in (3.13). Such a condition is not perfectly guaranteed when considering an approximate solution $\widehat{v}_{m,n}$, but, if the numerical approximation is accurate enough (i.e., for a cut-off index N large enough), the approximate denominator is close enough to the exact one, thus being nonzero. Observe that the same potentially critical issue occurs when directly using the Mathieu functions, as in [14]; in that case the degree of the involved Mathieu functions must be large enough, in analogy with the present one.

Let us summarize the basic steps of the method we propose for solving the inverse problem. Given ν, a, b and given the T-periodic flow rate $f(t)$, we proceed as follows:

(S1) We consider an integer M such that the Fourier spectrum of $f(t)$ is suitably approximated by $\widehat{f}_m$ for $m \in \{0, 1, \dots, M\}$. To assess the accuracy of this choice it is possible to use popular metrics, such as the Pearson correlation coefficient; see [14].

(S2) Given M, we fix desired (small enough) thresholds $\bar{\mu}$, $\bar{s}$, and we determine $N^\star$ as in section 3.2. By the end of this step, the accurate and truncation-independent computation of the modes $\widehat{v}_{m,n}$ is achieved for $m \in \{0, 1, \ldots, M\}$ and $n \in \{0, 2, \ldots, 2N^\star\}$.

(S3) Given $\widehat{v}_{m,n}$, we use (3.13) to compute $\widehat{\lambda}_m$; by the end of this step, the coefficients $\widehat{\lambda}_m$ are available, for $m \in \{0, 1, \ldots, M\}$.

(S4) We compute the sought approximate solution by replacing (3.5) with the following summation:

(3.14)
$$u(t,\eta,\theta) \cong \sum_{m\in\bar{\mathcal{M}}} \widehat{\lambda}_m\, \varphi_m(\eta,\theta)\, e^{i\omega_m t}, \quad \text{with} \quad \varphi_m(\eta,\theta) = \sum_{n\in\bar{\mathcal{N}}^\star} \widehat{v}_{m,n}(\eta)\, e^{in\theta},$$

where $\bar{\mathcal{M}} = \{-M, -M+1, \ldots, M-1, M\}$ and $\bar{\mathcal{N}}^\star = \{-2N^\star, -2N^\star + 2, \ldots, 2N^\star - 2, 2N^\star\}$, where the modes associated with negative values of m and n are evaluated by conjugacy.

We observe that at step (S2) we need to solve system (3.9) for several values of N. However, this burden is not peculiar to our strategy: It is necessary to iterate computations also when directly using the Mathieu functions, to reach a proper accuracy level [14]. Next, let us remark that if one addresses multiple flow rates $f_i(t)$ on the same cross section, it suffices to determine $N^\star$ by considering $M = \max_i\{M_i\}$, thus performing step (S2) only once, to reduce the computational burden. Indeed, once the "basis" $\widehat{v}_{m,n}$ is built, it is immediate to explore many solutions, by simply iterating steps (S3)–(S4) on the given sets of coefficients $\widehat{f}_m$.

4. Numerical results. The proposed method was tested on blood and cerebrospinal fluid (CSF) flow, with the main aim of assessing its computational gain versus numerical approaches based on commercial codes, as well as its capability to deal with strongly elliptical cross sections. Both these aspects are discussed in section 5, based on the results from the present section. We remark that, although considering physiological data, we do not claim our tests to be very representative from a physiological viewpoint, since fully developed flows can hardly occur in real situations.

4.1. Blood flow in the internal carotid artery. A flow rate waveform for blood flow within the human internal carotid artery (ICA) was adapted from [17] (see Figure 4.1); the period is $T = 0.95$ (s), and the period-averaged flow rate is $f_0 = 4.11$ (cm^3/s). Following [19], an average radius for such a vessel is 0.25 (cm). By assuming $\varepsilon = 0.6$, we introduced an elliptical cross section with semiaxes $\alpha = 0.25$ (cm) and $\beta = 0.15$ (cm), so that $\eta \in E'_\eta = [0, b]$ with $b = 0.69$. A characteristic diameter for the section is then $\tilde{\delta} = \alpha + \beta = 0.4$ (cm), while the section-averaged speed is $\bar{w} = f_0/A = 34.9$ (cm/s), where $A = \pi\alpha\beta$ is the cross-sectional area. Moreover, the flux was approximated by $M = 15$ modes suitably replacing the data (see Figure 4.1), since the associated Pearson correlation coefficient differs from 1 by less than 10^{-3}. By introducing a characteristic speed $\tilde{w} = A^{-1} \max_{t/T\in[0,1]} f(t) = 58.2$ (cm/s) and by assuming $\nu = 3.5 \cdot 10^{-2}$ (cm^2/s), as in [30], we label the considered blood flow with a Reynolds number $Re = \tilde{w}\tilde{\delta}/\nu \cong 665$. In addition, once a characteristic frequency $\widetilde{\omega} = \big(\sum_{m=0}^{M} |\widehat{f}_m|\, \omega_m\big) / \big(\sum_{m=0}^{M} |\widehat{f}_m|\big)$ is defined, we introduce a characteristic Womersley number $\mathrm{Wo} = (\tilde{\delta}/2)\sqrt{\widetilde{\omega}/\nu} \cong 2.5$. Despite the scarcity of results on stability for pulsatile flows, which seem to be contradictory already for the circular cross section [34], the above values suggest that the flow at hand is laminar. This was derived

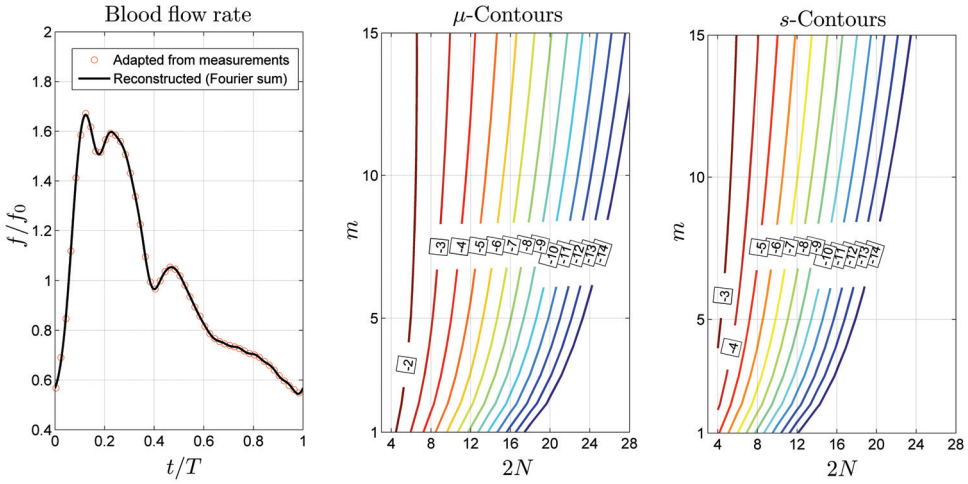

FIG. 4.1. *Blood flow within the ICA. Normalized flow rate f/f_0: Data, adapted from* [17]*, are plotted against a Fourier reconstruction with $M = 15$ modes (left). Contour plots for $\mu(m, N)$: It is necessary to choose $2N = 26$ for the relative magnitude of discarded modes to be below 10^{-12} for all considered m (middle). Contour plots for $s(m, N)$: It is necessary to choose $2N = 22$ to get a relative sensitivity to truncation below 10^{-12} for all considered m (right).*

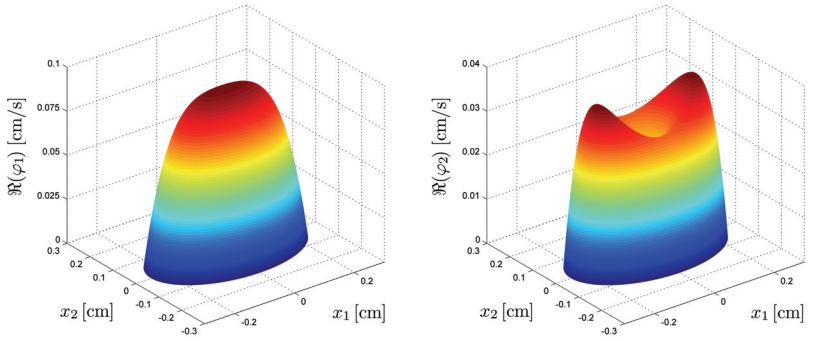

FIG. 4.2. *Blood flow within the ICA. Example solution components: Real part of φ_1 (left) and φ_2 (right).*

by considering available experimental thresholds for the circular cross section [15], due to the lack of more appropriate available criteria for the elliptical case. Step (S2) of the method was then addressed, thus obtaining the contours shown in Figure 4.1 for $\mu(m, N)$ and $s(m, N)$. For this purpose, we coded the boundary value problem (3.9) within a MATLAB environment and solved it by a shooting technique. As a result, by choosing $\bar{\mu} = \bar{s} = 10^{-12}$, it is immediate to get $N^\star_{\bar{\mu}} = 13$ and $N^\star_{\bar{s}} = 11$ from Figure 4.1, so as to finally choose $N^\star = 13$. Please also notice how, for any fixed m, $\|\widehat{v}_{m,n}\|_\infty \geq \|\widehat{v}_{m,n+2}\|_\infty$ for $n = 0, \ldots, 2N-2$, thus confirming the decreasing influence of higher n-modes. Furthermore, Figure 4.2 shows the real part of φ_1 and φ_2, defined in (3.14), for the sake of illustration.

We then compared our numerical results with those achieved by means of the commercial finite element (FE) solver ADINA 8.8.1 (ADINA R&D Inc., MA, USA). Such a solver uses a standard Galerkin formulation (stabilized by upwinding for higher Reynolds numbers [3]), while time-advancing is implemented by a first order Euler

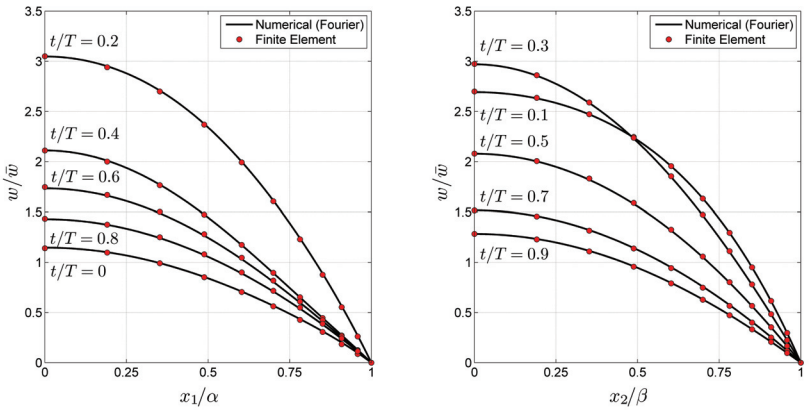

FIG. 4.3. *Blood flow within the ICA. Normalized velocity profiles $w/\bar{w}$ along the major (left) and minor (right) semiaxes, for selected nondimensional times t/T. Results obtained by the proposed method (solid curves) are compared with those achieved by a commercial FE solver (filled circles).*

backward method. In FE simulations, a pipe with length $\ell = 160\tilde{\delta}$ was defined, to obtain a fully developed flow in the central portion of the domain. (Such a condition was checked a posteriori.) Furthermore, the flow rate shown in Figure 4.1 was imposed at the inlet cross section, the no-slip boundary condition was enforced on the vessel wall, and a reference pressure value was imposed at the outlet cross section. (Such a value is immaterial, due to the incompressible formulation.) In addition, both space- and time-discretization were incrementally refined, up to obtaining discretization-independent results. In particular, the pipe domain was discretized by nearly $8.2 \cdot 10^5$ second order accurate brick elements, namely 20, 32, and 1280 elements along the radial, circumferential, and axial directions, respectively. Moreover, seven pulsation periods were simulated (time-periodicity was obtained after four periods); the time-step was internally set, based on the chosen 10^{-5} relative tolerance on residuals. Finally, all simulations were run on a single core of a PC with Intel Core i7-960 3.20 GHz CPU and 24 GB RAM. As expected, a very good agreement was achieved between the considered approaches; see Figure 4.3. In particular, the root-mean-square (RMS) difference between the corresponding velocities was $\Delta w \cong 4.2 \cdot 10^{-3}\,\tilde{w}$. Associated computational times were noticeably different: Roughly 3 minutes for the proposed method, versus 9 days for the FE run.

4.2. Cerebrospinal fluid flow in the upper cervical spinal region. A flow rate waveform for CSF in the upper cervical human spinal region [18] was adapted from [14]. The period-averaged flow rate is $f_0 = -0.11$ (cm^3/s). (Negative sign indicates that it is directed towards the lumbar region.) The period $T = 0.95$ (s) was assumed equal to that of the cardiac cycle; see section 4.1. The cross section can be approximated by the annulus between two confocal ellipses with $\alpha_2 = 1.11$ (cm), $\beta_2 = 0.93$ (cm), and $\beta_1 = 0.43$ (cm) (from which $a = 0.61$ (cm) and $\alpha_1 = 0.74$ (cm)), so that $\eta \in E' = [b_1, b_2]$ with $b_1 = 0.66$ and $b_2 = 1.21$. A characteristic thickness for the cross section is $\tilde{\tau} = (\alpha_2 - \alpha_1 + \beta_2 - \beta_1)/2 = 0.43$ (cm), while the section-averaged speed is $\bar{w} = f_0/A = -0.047$ (cm/s), where A represents the cross-sectional area. The flux was approximated by $M = 15$ modes suitably replacing the data (see Figure 4.4), since the associated Pearson correlation coefficient differs from 1 by less than 10^{-6}. Moreover, by proceeding as in section 4.1 with $\tilde{\tau}$ in place of $\tilde{\delta}$, and

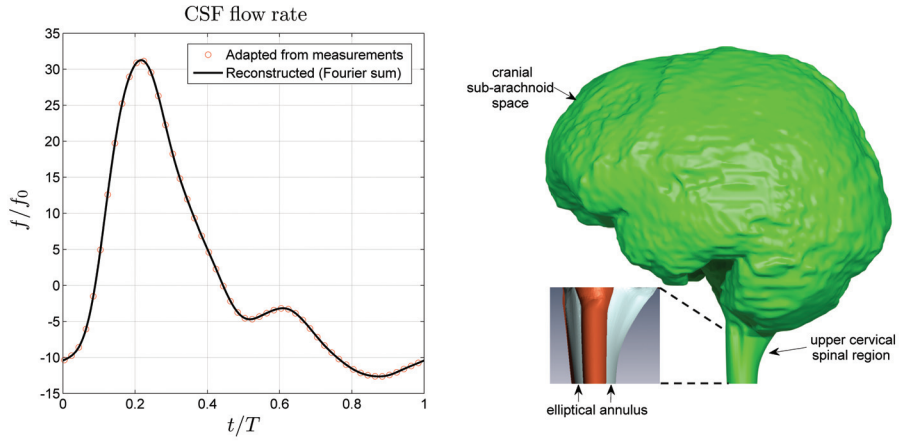

FIG. 4.4. *CSF flow in the upper cervical spinal region. Normalized flow rate f/f_0: Data adapted from* [14] *are plotted against Fourier reconstruction based on $M = 15$ modes (left). 3D Reconstruction of a patient-specific CSF domain, as obtained from MRI, showing cranial sub-arachnoid space and upper cervical spinal region (right). Location of the considered annulus is highlighted in the inset.*

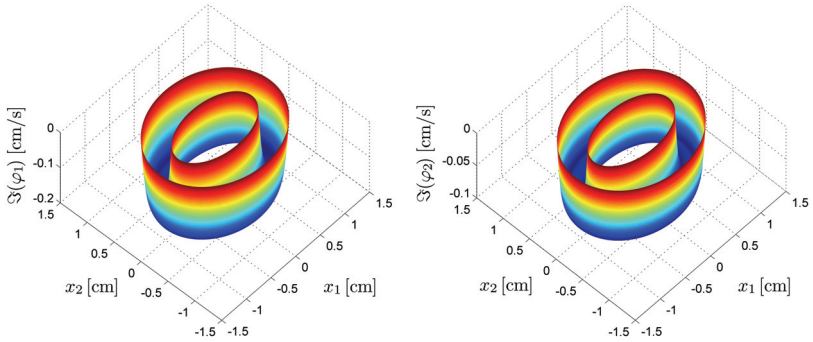

FIG. 4.5. *CSF flow in the upper cervical spinal region. Example solution components: Imaginary parts of φ_1 (left) and φ_2 (right).*

by assuming $\nu = 10^{-2}$ (cm^2/s), as in [22], we label the considered blood flow with a Reynolds number $Re = \tilde{w}\tilde{\tau}/\nu \cong 65$ and a Womersley number $\mathrm{Wo} = (\tilde{\tau}/2)\sqrt{\tilde{\omega}/\nu} \cong 7.5$. The above values suggest that the flow at hand is laminar, yet also in this case more consolidated results are needed for a stronger statement on stability (available data do not consider annular sections [34]). We then determined $N^\star = 13$, once $\bar{\mu} = \bar{s} = 10^{-12}$ was chosen. Figure 4.5 shows the imaginary part of φ_1 and φ_2, for the sake of illustration. We then compared our numerical results with those achieved by the commercial solver ADINA. For such FE simulations, a pipe with length $\ell \cong 100\bar{\tau}$ was defined, in order to obtain a fully developed flow in the central portion of the domain. The flow rate shown in Figure 4.4 was imposed at the inlet cross section, the no-slip boundary condition was enforced on vessel walls, and a reference pressure value was imposed at the outlet cross section. Also in this case space- and time-discretization were incrementally refined. The pipe domain was finally discretized by nearly $3.8 \cdot 10^5$ second order accurate brick elements, namely 40, 32, and 300 elements along the radial, circumferential, and axial directions, respectively. Moreover, seven

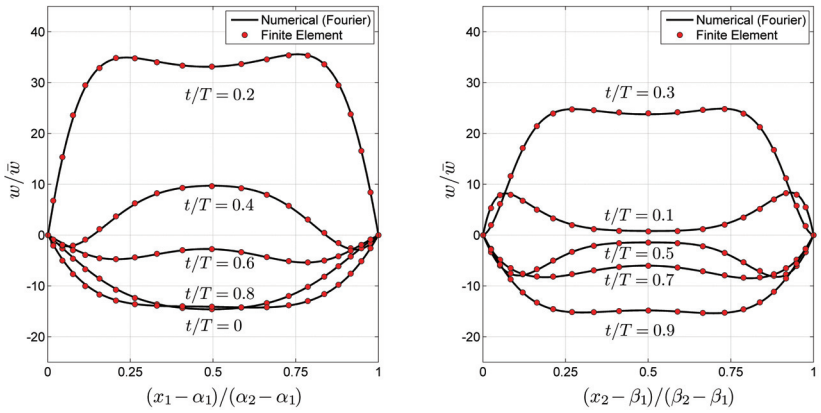

FIG. 4.6. *CSF flow in the upper cervical spinal region. Normalized velocity profiles $w/\bar{w}$ along the major (left) and minor (right) semiaxes of the annulus, for selected nondimensional times t/T. Results obtained by the proposed Fourier-based approach (solid curves) are compared with those achieved by a commercial FE solver (filled circles).*

pulsation periods were simulated (time-periodicity was obtained after two periods), and a time-step was internally set, once a 10^{-5} relative tolerance on the residuals was chosen. Also in this case, a very good agreement was achieved between the considered approaches (see Figure 4.6), the RMS difference between the corresponding velocities being $\Delta w \cong 4.5 \cdot 10^{-3}\,\tilde{w}$. Associated computational times were noticeably dissimilar: Roughly 3 minutes for the proposed method, versus 4 days for the FE run (the latter being shorter than in the blood test-case, thanks to lower average speeds).

5. Discussion and concluding remarks. We proposed a novel numerical method for solving the inverse problem of fully developed pulsatile viscous flows of an incompressible Newtonian fluid in elliptical vessels and annuli between confocal ellipses. Under quite general assumptions, valuable approaches for problems with flow rate conditions were proposed in the literature [11], and they are the subject of ongoing research. Moreover, a fully numerical approach is the only one viable when considering realistic geometries and complex rheology; nonetheless and in spite of the linear context within which it was derived, our solution is original and nontrivial. Indeed, it provides an easily computable benchmark, as well as an approximation, for such a problem. We successfully applied the method to blood and CSF flows; in both cases, the solution provided by a commercial numerical solver was accurately reproduced in a much shorter computational time. Indeed, the corresponding speed-up factor was over 10^3, and it could be enhanced by using optimized Fourier solvers [13]. Please also notice that it takes additional time to get a grid-independent, periodic, and fully developed FE solution (such time was not considered in section 4), so that actual computational gain was even greater.

More generally, our method corroborates some early attempts in which a proper treatment of the inverse problem was missing [29], and it provides an alternative to the numerical approach in [14], heavily based on Mathieu functions. As regards computational time, our approach seems to be comparable to that in [14]. However, to optimize computational efficiency was not our main intent (so that we did not reproduce the computations in [14]); rather we were looking for a method able to also deal with strongly elliptical sections, where the approach based on Mathieu functions

is reported to face difficulties [16]. We thus challenged our strategy by varying the cross sections adopted for the numerical test-cases in section 4. In particular, once the given flow rate and the cross-sectional area were fixed, we considered many sections by assigning the ellipticity parameter ε, namely β/α for the ellipse and β_2/α_2 for the annulus. More precisely, for the annular case we fixed the cross-sectional area of both ellipses, and the resulting section was completely defined also thanks to the confocality condition. No criticalities were encountered by our method, even for $\varepsilon < 0.1$. Example results are reported in Figure 5.1, where nondimensional velocity profiles can be directly compared since $\bar{w}$ was kept constant while varying ε. For the considered blood flow within the ICA, pulsation does not play a major role (due to a smaller Womersley number), and the velocity profiles are somehow scaled with the flow rate (see Figure 4.3), with a slight exception around $t/T = 0.1$. In such a circumstance one expects the instantaneous velocity profiles to almost behave as in the stationary case: Ellipticity indirectly enters through the space variable scaling in (2.7), so that the nondimensional velocity profiles are expected to be weakly dependent on ε. This was confirmed by our simulations, and minor deviations could only be observed for $t/T = 0.1$; see Figure 5.1. Conversely, pulsatility is more pronounced for the considered CSF flow (with a larger Womersley number), and ellipticity sensibly affects the nondimensional velocity profiles, as shown in Figure 5.1. It is easy to check that for smaller ε both thicknesses $\alpha_2 - \alpha_1$ and $\beta_2 - \beta_1$ are decreasing in ε, so that viscosity effects become more relevant and there is only one maximum for the velocity profiles as in the parabolic case. In more detail, $\alpha_2 - \alpha_1$ tends to zero, and the corresponding velocity profile is almost completely damped, while $\beta_2 - \beta_1$ tends to a nonnull value, so that the corresponding velocity profile is also determined by mass continuity (see Figure 5.1 for $\varepsilon = 0.1$). Hence, vessel ellipticity affects the solution, and for larger Womersley numbers it is not possible to simply scale the spatial variables. Indeed, in those cases it is necessary to properly solve the inverse problem, e.g., by using the approach in [14] or the one proposed in the present study, yet our method seems to be preferable for strongly elliptical cross sections.

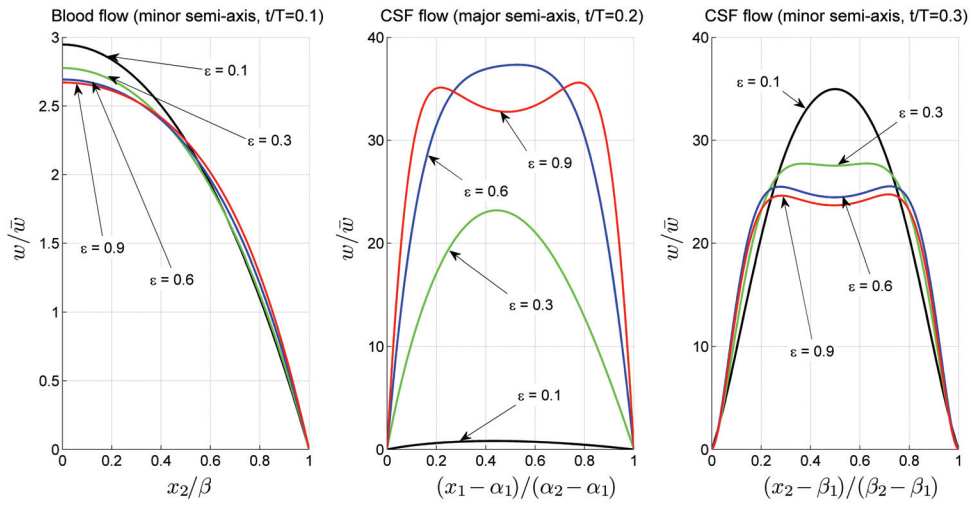

FIG. 5.1. *Effect of the ellipticity parameter ε on fluid velocity. Example nondimensional velocity profiles for blood (left) and CSF (middle and right) flows.*

Nonetheless, the applicability of our method to real-world test-cases is limited by the underlying assumptions, primarily that of having a fully developed flow. The implications of such an assumption on model usability could be addressed by quantifying the degree of approximation of our solution compared to finite-length vessel flows. In this regard, it could be of interest to study the "entrance length" for pulsatile and for purely oscillatory flows in both elliptical pipes and annuli, also considering outflow boundary conditions as in [35]. Furthermore, the proposed method cannot be applied to nonconfocal elliptical annuli, and it cannot take into account relevant features of realistic vessels such as curvature [2], twist, and taper. Further aspects, such as the possibility of accurately measuring vessel ellipticity in patient-specific geometries, also affects model applicability. In addition, it may be appropriate to consider more complex fluid rheological aspects, especially for blood flow [28]. Finally and more importantly, the proposed model does not address compliance of the vessel walls, which can strongly affect the solution for both CSF and blood flows [8, 7]. Indeed, the relative importance of ellipticity and wall compliance should be better studied, to obtain accurate predictions of the wall shear stress distribution along the cross section boundary, which in turn can affect the onset and development of relevant blood- and CSF-related pathologies. As anticipated, however, investigation of physiologically relevant near-wall conditions and transport phenomena was beyond the present scope, and it will be tackled through subsequent studies.

Despite the aforementioned limitations, the proposed method can be effectively used for developing more ambitious numerical studies, e.g., as an improved source of initial/boundary data, up to serving as a debugging tool for complex 3D codes. Indeed, our benchmark solution can provide a more appropriate flow field when pulsatility plays a role, thus improving those approaches which only scale the parabolic velocity profile by a factor accounting for flow rate variability. Besides basic biofluid dynamics investigations, our method can be applied to many problems in the biomedical field such as targeted drug delivery [5] and controlled navigation of so-called "medical microrobots" [24], for which blood and CSF were identified as elective carrying fluids. In both applications, our method could provide a more precise description of the underlying flow field, still at an affordable computational cost, which is needed to improve the accuracy of drug/microdevice release and targeting. Furthermore, regarding CSF flow, improved flow description could permit us to better assess glucose transport, which is envisioned for powering implantable miniaturized electronic devices [25]. In conclusion, we believe that the proposed method, despite the simplifications that we introduced for obtaining a directly computable solution, has potential for effective applications in an interdisciplinary context.

Acknowledgments. The authors would like to thank Costanza Diversi and Byung-Jeon Kang for the 3D reconstruction reported in Figure 4.4.

REFERENCES

[1] F. A. Alhargan, *A complete method for the computations of Mathieu characteristic numbers of integer orders*, SIAM Rev., 38 (1996), pp. 239–255.

[2] N. Arada, M. Pires, and A. Sequeira, *Viscosity effects on flows of generalized Newtonian fluids through curved pipes*, Comput. Math. Appl., 53 (2007), pp. 625–646.

[3] K. J. Bathe, H. Zhang, and M. H. Wang, *Finite element analysis of incompressible and compressible fluid flows with free surfaces and structural interactions*, Comput. Struct., 56 (1995), pp. 193–213.

[4] H. Beirão da Veiga, *Time periodic solutions of the Navier-Stokes equations in unbounded cylindrical domains—Leray's problem for periodic flows*, Arch. Ration. Mech. Anal., 178 (2005), pp. 301–325.
[5] L. C. Berselli, P. Miloro, A. Menciassi, and E. Sinibaldi, *Exact solution to the inverse Womersley problem for pulsatile flows in cylindrical vessels, with application to magnetic particle targeting*, Appl. Math. Comput., 219 (2013), pp. 5717–5729.
[6] L. C. Berselli and M. Romito, *On Leray's problem for almost periodic flows*, J. Math. Sci. Univ. Tokyo, 19 (2012), pp. 69–130.
[7] C. D. Bertram, *A numerical investigation of waves propagating in the spinal cord and subarachnoid space in the presence of a syrinx*, J. Fluids Struct., 25 (2009), pp. 1189–1205.
[8] S. Čanić, J. Tambača, G. Guidoboni, A. Mikelić, C. J. Hartley, and D. Rosenstrauch, *Modeling viscoelastic behavior of arterial walls and their interaction with pulsatile blood flow*, SIAM J. Appl. Math., 67 (2006), pp. 164–193.
[9] S. Cheng, M. A. Stoodley, J. Wong, S. Hemley, D. F. Fletcher, and L. E. Bilston, *The presence of arachnoiditis affects the characteristics of CSF flow in the spinal subarachnoid space: A modelling study*, J. Biomech., 45 (2012), pp. 1186–1191.
[10] C. Di Rocco, P. Frassanito, L. Massimi, and S. Peraio, *Hydrocephalus and Chiari type* I *malformation*, Childs Nerv. Syst., 27 (2011), pp. 1653–1664.
[11] L. Formaggia, A. Veneziani, and C. Vergara, *Flow rate boundary problems for an incompressible fluid in deformable domains: Formulations and solution methods*, Comput. Methods Appl. Mech. Engrg., 199 (2010), pp. 677–688.
[12] G. P. Galdi and A. M. Robertson, *The relation between flow rate and axial pressure gradient for time-periodic Poiseuille flow in a pipe*, J. Math. Fluid Mech., 7 (2005), pp. S215–S223.
[13] L. Greengard and J.-Y. Lee, *Accelerating the nonuniform fast Fourier transform*, SIAM Rev., 46 (2004), pp. 443–454.
[14] S. Gupta, D. Poulikakos, and V. Kurtcuoglu, *Analytical solution for pulsatile viscous flow in a straight elliptic annulus and application to the motion of the cerebrospinal fluid*, Phys. Fluids, 20 (2008), 093607.
[15] K. Haddad, O. Ertunç, M. Mishra, and A. Delgado, *Pulsating laminar fully developed channel and pipe flows*, Phys. Rev. E, 81 (2010), 016303.
[16] M. Haslam and M. Zamir, *Pulsatile flow in tubes of elliptic cross sections*, Ann. Biomed. Eng., 26 (1998), pp. 780–787.
[17] Y. Hoi, B. A. Wasserman, Y. Y. J. Xie, S. S. Najjar, L. Ferruci, E. G. Lakatta, G. Gerstenblith, and D. A. Steinman, *Characterization of volumetric flow rate waveforms at the carotid bifurcations of older adults*, Physiol. Meas., 31 (2010), pp. 291–302.
[18] D. N. Irani, *Cerebrospinal Fluid in Clinical Practice*, Saunders, Philadelphia, 2008.
[19] J. Krejza, M. Arkuszewski, S. E. Kasner, J. Weigele, A. Ustymowicz, R. W. Hurst, B. L. Cucchiara, and S. R. Messe, *Carotid artery diameter in men and women and the relation to body and neck size*, Stroke, 37 (2006), pp. 1103–1105.
[20] M.-C. Lai, *Fast direct solver for Poisson equation in a 2D elliptical domain*, Numer. Methods Partial Differential Equations, 20 (2004), pp. 72–81.
[21] A. A. Linninger, M. Xenos, B. Sweetman, S. Ponkshe, X. Guo, and R. Penn, *A mathematical model of blood, cerebrospinal fluid and brain dynamics*, J. Math. Biol., 59 (2009), pp. 729–759.
[22] F. Loth, M. A. Yardimci, and N. Alperin, *Hydrodynamic modeling of cerebrospinal fluid motion within the spinal cavity*, J. Biomech. Eng., 123 (2001), pp. 71–79.
[23] N. W. McLachlan, *Theory and Application of Mathieu Functions*, Clarendon Press, Oxford, UK, 1947.
[24] B. J. Nelson, I. K. Kaliakatsos, and J. J. Abbott, *Microrobots for minimally invasive medicine*, Annu. Rev. Biomed. Eng., 12 (2010), pp. 55–85.
[25] B. I. Rapoport, J. T. Kedzierski, and R. Sarpeshkar, *A glucose fuel cell for implantable brain-machine interfaces*, PLoS ONE, 7 (2012), e38436.
[26] Y. V. K. Ravi Kumar, P. S. V. H. N. Krishna Kumari, M. V. Ramana Murthy, and S. Sreenadh, *Unsteady peristaltic pumping in a finite length tube with permeable wall*, J. Fluids Eng., 132 (2010), 101201.
[27] S. Ray and F. Durst, *Semianalytical solutions of laminar fully developed pulsating flows through ducts of arbitrary cross sections*, Phys. Fluids, 16 (2004), pp. 4371–4385.
[28] A. M. Robertson, A. Sequeira, and R. G. Owens, *Rheological models for blood*, in Cardiovascular Mathematics, Model. Simul. Appl. 1, Springer Italia, Milan, 2009, pp. 211–241.
[29] M. B. Robertson, U. Köhler, P. R. Hoskins, and I. Marshall, *Flow in elliptical vessels calculated for a physiological waveform*, J. Vasc. Res., 38 (2001), pp. 73–82.

[30] K. Rogers, *Blood: Physiology and Circulation*, Human Body series, Rosen Publishing Group, New York, 2010.
[31] T. Sexl, *Uber den von E. G. Richardson entdeckten "Annulareffekt"*, Z. Phys, 61 (1930), pp. 179–221.
[32] N. Shaffer, B. Martin, and F. Loth, *Cerebrospinal fluid hydrodynamics in type* I *Chiari malformation*, Neurol. Res., 33 (2011), pp. 247–260.
[33] J. Shen and L.-L. Wang, *On spectral approximations in elliptical geometries using Mathieu functions*, Math. Comp., 78 (2009), pp. 815–844.
[34] R. Trip, D. J. Kuik, J. Westerweel, and C. Poelma, *An experimental study of transitional pulsatile pipe flow*, Phys. Fluids, 24 (2012), 014103.
[35] A. Veneziani and C. Vergara, *An approximate method for solving incompressible Navier-Stokes problems with flow rate conditions*, Comput. Methods Appl. Mech. Engrg., 196 (2007), pp. 1685–1700.
[36] P. D. Verma, *The pulsating viscous flow superposed on the steady laminar motion of incompressible fluid between two co-axial cylinders*, Proc. Indian Acad. Sci. Math. Sci., 26 (1960), pp. 447–458.
[37] P. D. Verma, *The pulsating viscous flow superposed on the steady laminar motion of incompressible fluid in a tube of elliptic section*, Proc. Indian Acad. Sci. Math. Sci., 26 (1960), pp. 282–297.
[38] J. R. Womersley, *Method for the calculation of velocity, rate of flow and viscous drag in arteries when the pressure gradient is known*, J. Physiol., 127 (1955), pp. 553–563.